A Class-E Direct Ac-Ac Converter with Multi-Cycle Modulation for Induction Heating Systems

Abstract- **Induction heating systems are the technology of choice in many industrial, domestic and medical applications due to its high performance. The core component of such systems is the power supply, which is usually composed of a rectifier stage and a resonant inverter. In order to simplify and further optimize the performance of the power supply, a class-E direct ac-ac converter featuring multi-cycle modulations is proposed in this paper.**

The proposed converter is composed of two switching devices that enable the direct ac-ac conversion. Single and multi-cycle operation modes have been analytically described to prove the benefits in terms of peak voltage reduction and output power control capabilities. A prototype featuring SiC JFET devices, which perfectly fit these applications, has been designed and built to prove the feasibility of the proposed converter. The experimental results match the analytical ones and validate the benefits of this converter.

I. INTRODUCTION

The induction heating (IH) technology is based on the generation of a high frequency magnetic field by the application of high current levels through an inductor (Fig. 1). As a result, the material can be directly heated, avoiding physical contact between source and generator. IH technology has experienced a significant growth in recent years due to its benefits in terms of reliability, performance [1] and safety when compared with other heating technologies. The availability of high-performance, reliable, and cost-effective equipment has multiplied the applications of IH systems in the industrial, domestic, and health spheres.

Advances in power electronics have enabled in the last decade the design of high performance power supplies for IH systems, leading to a significant breakthrough in IH technology. The main building blocks of an IH power supply are a rectifier and a high frequency inverter, which supplies the required current to the induction heating load in order to generate an alternating magnetic field. It induces eddy currents in the surface of the material under treatment, leading to resistive losses that heat up the induction target.

Different resonant converter topologies [2] have been proposed depending on the required output power and final applications. On one hand, single-switch quasi-resonant inverters, usually based on the class-E converter [3], have been widely used for low-power induction systems that feature constant induction heating load. The main advantage of this topology is its simplicity and low cost, whereas the limited output power and control capabilities are its main drawbacks. On the other hand, full [4-7] and half-bridge [8-12] resonant inverters, also called class-D converters, have been proposed for high-medium output power levels. Those topologies feature higher output power capabilities and improved power control with increased complexity and cost. In addition to this, some specific topologies have been proposed for specific purposes such as multi-inductor [13-16], high-efficiency [17], or selectable induction heating target systems [18, 19].

This paper proposes a class-E quasi-resonant direct ac-ac converter featuring multi-cycle modulations (MCMs) for IH systems. The main benefits of the proposed converter derive from the direct ac-ac conversion and the multi-cycle modulations. Firstly, direct ac-ac conversion allows removing the rectifier stage, reducing the number of components and its associated conduction losses. Secondly, multi-cycle modulation schemes allow reducing peak voltage and switching frequency, improving the operating conditions and output power control. The proposed converter has been tested using SiC JFET devices, proving its feasibility. As a conclusion, the proposed converter improves the performance and efficiency of induction heating systems in the low-medium output power range.

This paper is organized as follows. Section II presents the proposed class-E direct ac-ac converter and its basic operation mode. Multi-cycle modulation is presented in Section III, analyzing its benefits in terms of peak voltage and output power control. Section IV shows the main experimental results used to prove the feasibility of the proposed converter and, finally, the conclusions of this paper are drawn in Section V.

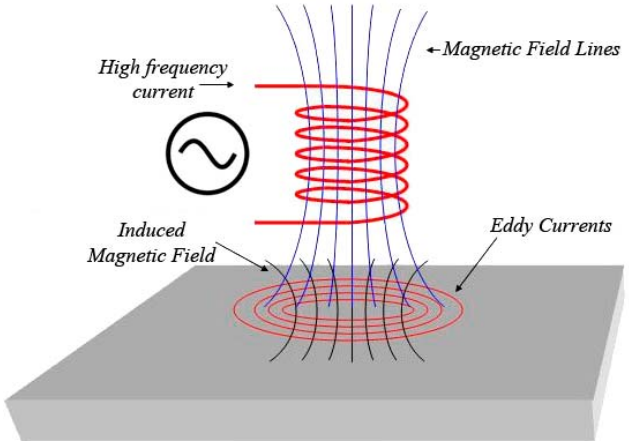

Fig. 1. Diagram of the induction heating phenomena.

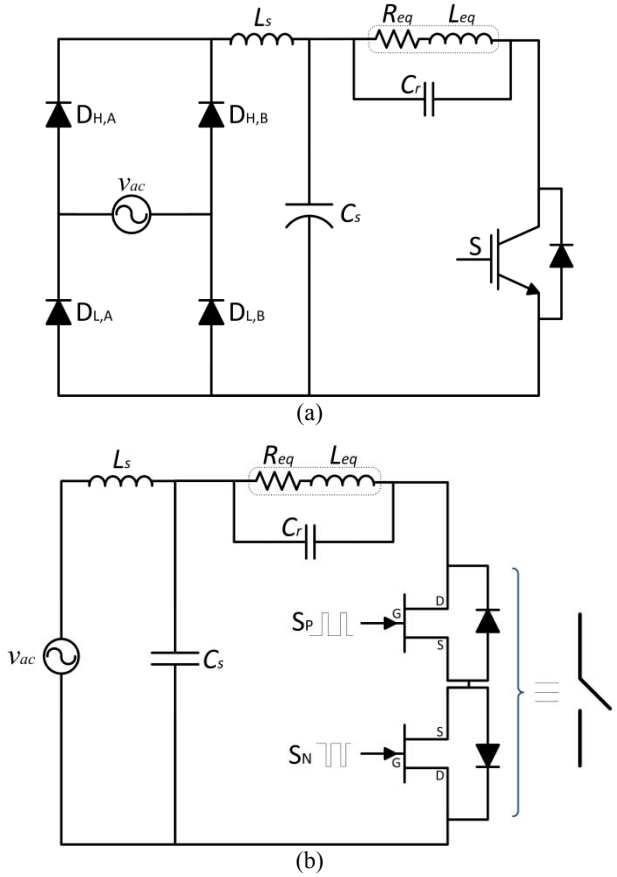

Fig. 2. Single switch ZVS converter. Classical implementation based on a full-bridge rectifier (a). Proposed implementation based on a bidirectional and bipolar equivalent switching device (b).

II. Description Of The Proposed Converter

Classical implementations of quasi-resonant single-switch ZVS converters for IH applications (Fig. 2.a) employ a bidirectional and unipolar switching device (S), typically a MOSFET/IGBT with antiparallel diode [20]. The mains ac voltage, V_{ac}, is rectified by means of a diode rectifier, and filtered by the series inductance L_s and the dc-link capacitor C_s. The resonant tank is composed of the induction heating load, modeled as a series resistance, R_{eq}, and inductance, L_{eq} [21, 22], and an additional resonant capacitor, C_r.

Unlike classical implementations [23-25], the converter proposed in this paper uses a four quadrants equivalent switching device composed of two transistors connected in anti-series (Fig. 2 (b)). Due to the high voltage requirements, SiC n-channel normally-off JFETs have been selected as switching devices in order to increase efficiency based on its low on resistance. As a result, the full-bridge diode rectifier is no longer needed, reducing conduction losses and the input filter requirements. As it will be proved in next section, the complexity added by increasing the number of switching devices is justified by the performance improvements.

The low on-state resistance of the SiC JFET increases efficiency whereas the fast switching times enable high operation frequencies, reducing components size. Moreover, optimized control strategies allow improving the converter behavior, especially when operating in multi-load systems typical of IH technology.

A. Analysis of the converter

Considering the converter switching frequency higher than the input mains frequency, the proposed direct ac-ac converter (Fig. 2 (b)) analysis can be simplified by assuming a constant positive supply voltage, V_s, and complementary results are obtained for negative mains voltage. Thus, the equivalent constant supply voltage considered for the analysis, V_s, is the rms value of the filtered mains ac voltage, $V_{ac,rms}$. In this analysis, the effect of the input filter will be neglected.

Two different circuit configurations are considered for this converter (Fig. 3). When the switching device conducts (State I) the equivalent circuit is a series RL. In this state, the resonant capacitor is short-circuited to the supply voltage source, and thus

$$v_c(t) = V_s, \ \left(0 \le t \le DT_{sw}\right). \tag{1}$$

The load current, i_o, results

$$i_o(t) = \frac{V_s}{R_{eq}} - \left(\frac{V_s}{R_{eq}} - I_A\right) e^{-\frac{R_{eq}}{L_{eq}}t}, \ \left(0 \le t \le DT_{sw}\right). \tag{2}$$

Where I_A, is the initial load current value, and I_B represents the final load current at $t=DT_{sw}$, for state I, D is the duty cycle, and DT_{sw} is the time length of State I. When the switching device is turned off, State II, the equivalent circuit is a RLC circuit composed of the electrical equivalent of the induction heating load and the resonant capacitor. Equation (3) express a family of solutions [26] of the differential equation that describes the resonant capacitor voltage

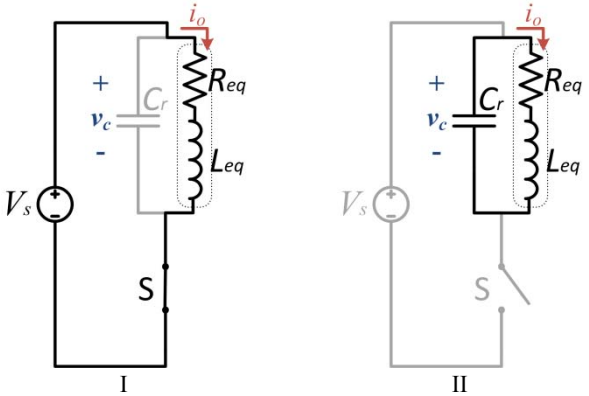

Fig. 3. Equivalent circuit states for the proposed converter.

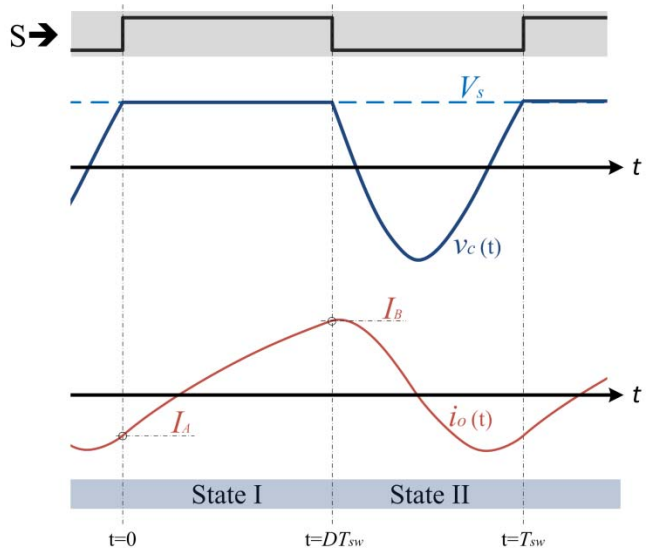

Fig. 4. Main waveforms of the proposed converter. From top to bottom: equivalent switch activation signal, resonant capacitor voltage and equivalent inductance current.

$$v_c(t) = e^{-\xi(t-DT_{sw})}\begin{pmatrix} k_1 \sin(\omega_n(t-DT_{sw}))+ \\ k_2 \cos(\omega_n(t-DT_{sw})) \end{pmatrix}, \left(DT_{sw} < t \le T_{sw}\right) \quad (3)$$

where $\xi = R_{eq}/2L_{eq}$ is the damping factor and $\omega_o = 1/\sqrt{L_{eq}C_r}$, $\omega_n = \sqrt{\omega_o^2 - \xi^2}$ are the resonant and natural angular frequencies, respectively. Thus, the load current, i_o, in State II results

$$i_o(t) = -C_r\frac{dv_c(t)}{dt} = $$

$$= C_r e^{-\xi(t-DT_{sw})}\begin{pmatrix} \sin(\omega_n(t-DT_{sw}))\left[V_s\omega_n + \xi k_1\right]+ \\ \cos(\omega_n(t-DT_{sw}))\left[V_s\xi - k_1\omega_n\right] \end{pmatrix}, \left(DT_{sw} < t \le T_{sw}\right). \quad (4)$$

Assuming a ZVS operation, four boundary conditions are established for the steady state condition, as it can be seen in Fig. 4:

$$\begin{cases} I_A = i_o(t = T_{sw}) \\ I_B = i_o(t = DT_{sw}) \\ V_s = v_C(t = T_{sw}) \\ V_s = v_C(t = DT_{sw}) \end{cases}. \quad (5)$$

By solving the inductor current restrictions two design conditions are obtained:

$$I_A = C_r e^{-\xi T_{sw}(1-D)}\begin{pmatrix} \sin(\omega_n T_{sw}(1-D))\left[k_2\omega_n + \xi k_1\right]+ \\ \cos(\omega_n T_{sw}(1-D))\left[k_2\xi - k_1\omega_n\right] \end{pmatrix}, \quad (6)$$

and replacing I_B from (2) at $t=DT_{sw}$, the second boundary condition results

$$\frac{V_s}{R_{eq}} - \left(\frac{V_s}{R_{eq}} - I_A\right)e^{-\frac{R_{eq}}{L_{eq}}DT_{sw}} = C_r\left(k_2\xi - k_1\omega_n\right). \quad (7)$$

Besides, by applying the resonant capacitor voltage restrictions (third and fourth boundary conditions), k_1 and k_2 results

$$k_1 = \frac{\left(e^{\xi(1-D)T_{sw}} - \cos(\omega_n(1-D)T_{sw})\right)}{\sin(\omega_n(1-D)T_{sw})}V_s, \quad (8)$$

$$k_2 = V_s. \quad (9)$$

Thus, the converter temporal waveforms are defined, and as a result, key converter parameters can be obtained. On the other hand, input power can be calculated by means of the average input current, I_s,

$$I_s = \frac{1}{T_{SW}}\int_0^{T_{SW}} i_s(t)dt = \frac{1}{T_{SW}}\int_0^{DT_{SW}} i_o(t)dt, \quad (10)$$

thus, the average input power, P, is

$$P = V_s I_s = \frac{V_s^2}{R_{eq}T_{sw}}\int_0^{DT_{sw}}\left[1 - \left(1 - \frac{I_A R_{eq}}{V_s}\right)e^{-2\xi t}\right]dt, \quad (11)$$

resulting

$$P = \frac{V_s^2}{R_{eq}T_{sw}}\left[DT_{sw} + \frac{1}{2\xi}\left(1 - \frac{I_A R_{eq}}{V_s}\right)\left(e^{-2\xi DT_{sw}} - 1\right)\right]. \quad (12)$$

As a result, Fig. 5 shows the normalized design plane for the proposed converter. A set of normalized parameters have been used to extend analytical results. Where $T_n = \omega_n T_{sw}$, is the normalized switching period, $P_n = P/\left(V_s^2/R_{eq}\right)$, represent the normalized input power, and $V_n = \hat{V}_{swtich}/V_s$, is the normalized switch peak voltage. The normalized output power as a function of control parameters (D, T_n) for different quality load quality factors, $Q = \omega_o L_{eq}/R_{eq}$, have been obtained. This diagram can be used to select the operating conditions to obtain a desired maximum output power with a maximum blocking voltage that is limited by the power device used.

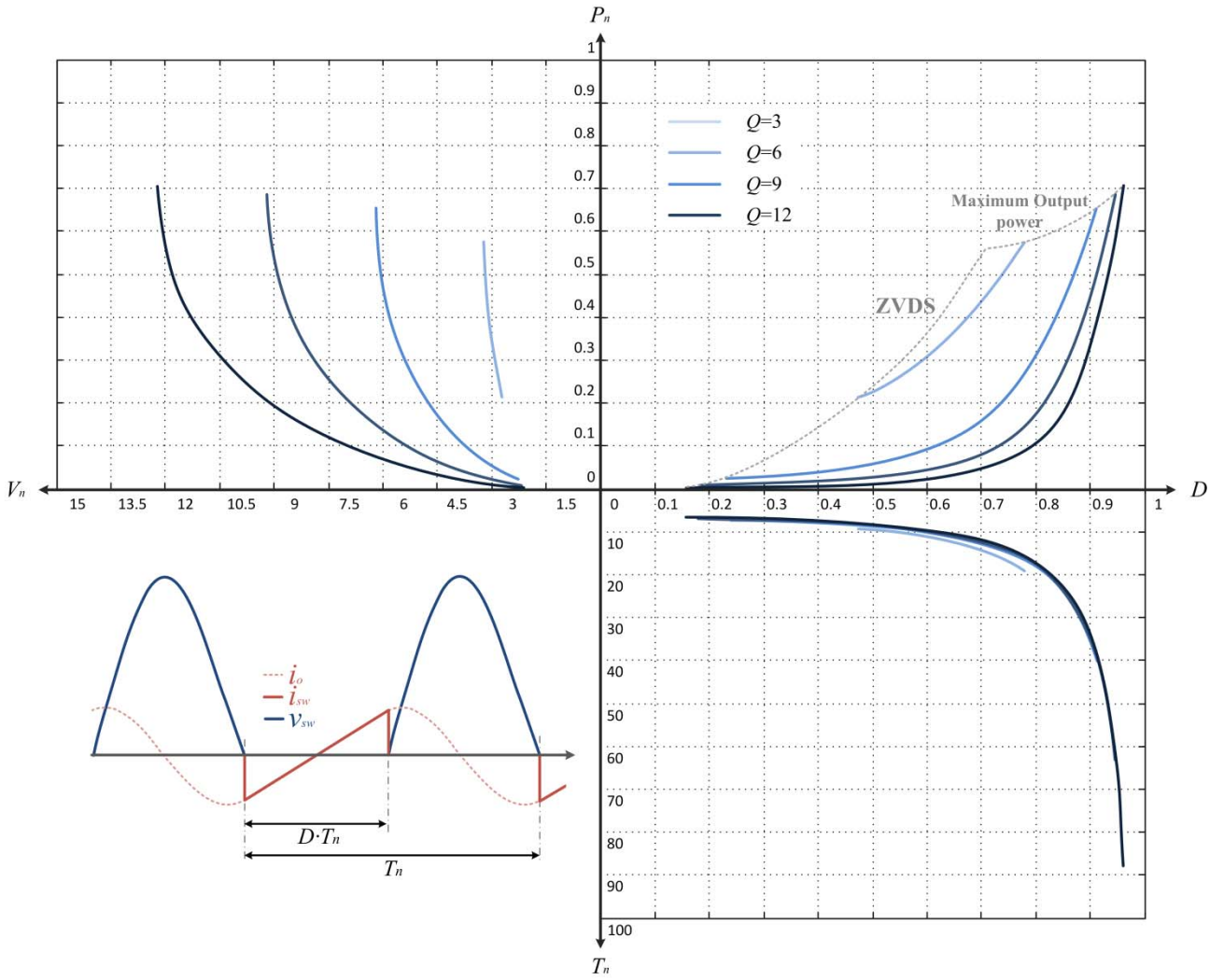

Fig. 5. Normalized design plane for the single-switch converter.

The classical implementation of the single-switch converter can be operated in optimum switching conditions, i.e. zero voltage switching (ZVS) and zero voltage derivative switching (ZVDS) for a single operation point, or in sub-optimum operation mode if only ZVS is satisfied.

Both operation modes are shown in Fig. 6. The optimum operation point is achieved at minimum duty cycle, where the minimum output power is delivered. In this operation mode, I_A=0, i.e. $i_o\big|_{t=0} = 0$, and $dv_s(t)/dt\big|_{t=0} = 0$ (ZVDS condition), and thus, switch current remains positive. On the other hand, for a given load, output power is increased if duty cycle is increased; in this situation (sub-optimum operation mode) I_A<0, and thus, the antiparallel diode starts conducting when device voltage reaches zero level. Consequently, the switching device is activated when antiparallel diode conducts, and thus, at zero voltage (ZVS); therefore, the turn-on soft-switching transition is guaranteed. In both operation modes, the resonant capacitor ensures a smooth turn-off transition. As a consequence, converter switching losses can be neglected.

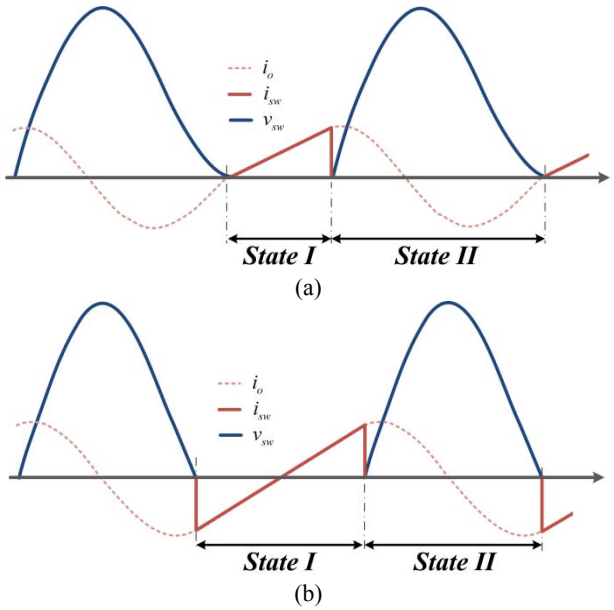

Fig. 6. Operation modes for the proposed converter. Optimum operation mode (a). Sub-optimum operation mode (b).

B. *Equivalent switching device*

The equivalent switching device S is composed of two series unipolar and bidirectional devices, S_P and S_N. For this implementation, SiC n-channel JFETs have been used. Although JFETs are selected, an antiparallel SiC diode has been added to protect switching device against negative drain-to-source voltage and ensure a smooth turn-on transition (Fig. 7 (a)). Depending on each switch activation, the equivalent switch conduction diagram changes according to Fig. 7 (b). Therefore, the equivalent switching device activation pattern can be expressed using a two-bit logic notation, i.e. one bit per series device activation, where the most significant bit denotes S_P activation (1 for activated, 0 for deactivated). Table I summarizes the equivalent switch activation notation.

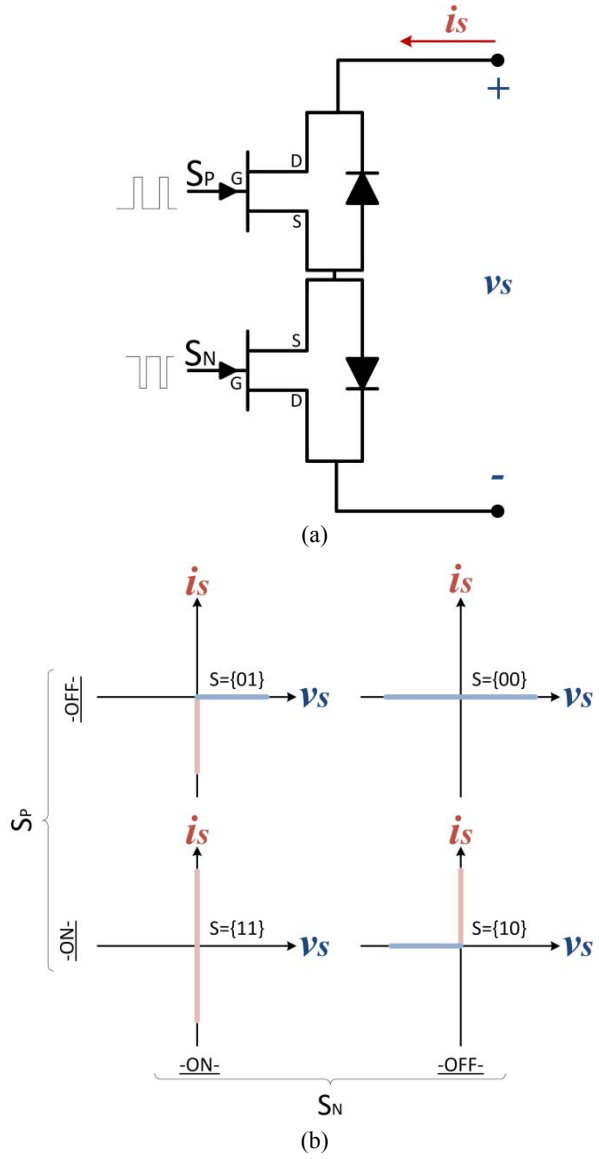

Fig. 7. Equivalent switch operation mode. Implementation schematic (a). Ideal conduction curves depending on both switch activation signals (b).

Table I
Equivalent Switching Device Activation

S_P	S_N	Equivalent switch logic activation	Conduction model
OFF	OFF	S={00}[25]	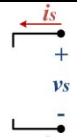
OFF	ON	S={01}	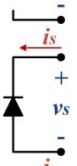
ON	OFF	S={10}	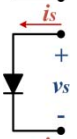
ON	ON	S={11}	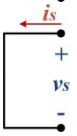

Hence, the equivalent switch can be operated as an ideal four-quadrant device (switch activation patterns {00}, {11}) or it can be operated as a device with unidirectional current conduction (activation pattern {10} for positive current and {01} for negative).

III. Multi-Cycle Modulation Schemes

By using the aforementioned properties of the four-quadrant equivalent switching device, a set of multi-cycle modulations (MCMs) can be achieved. MCMs are denoted as P_xN_y, where x denotes the number of positive half cycles and, y denotes the number of negative half cycles (Fig. 8). Using MCMs, sub-optimum ZVS switching conditions are guaranteed for each multi-cycle operation mode, and the optimum switching conditions, i. e. ZVS and ZVDS, are only achieved for P_xN_{x-1}, with $x \geq 1$. By the use of these MCMs, the device peak voltage to deliver the same output power can be reduced. In addition to this, the switching frequency is reduced, simplifying driver requirements, reducing switching losses, and enabling multi-load operation mode neglecting intermodulation noise between loads [11].

It is important to note that the number of times that the device voltage reaches zero results $m_z=x+y$; particularly for the case of optimum operation mode this number is odd, yielding $m_{z,opt}=2x-1$. The soft-switching ZVS turn-on process is guaranteed by the anti-parallel diode activation when its voltage becomes negative, and thus, it is required to adequately activate equivalent switching device to ensure the ZVS turn-on sequence. Fig. 9 shows the equivalent switching device activation pattern for different multi-cycle operation modes. In the case of the conventional single-

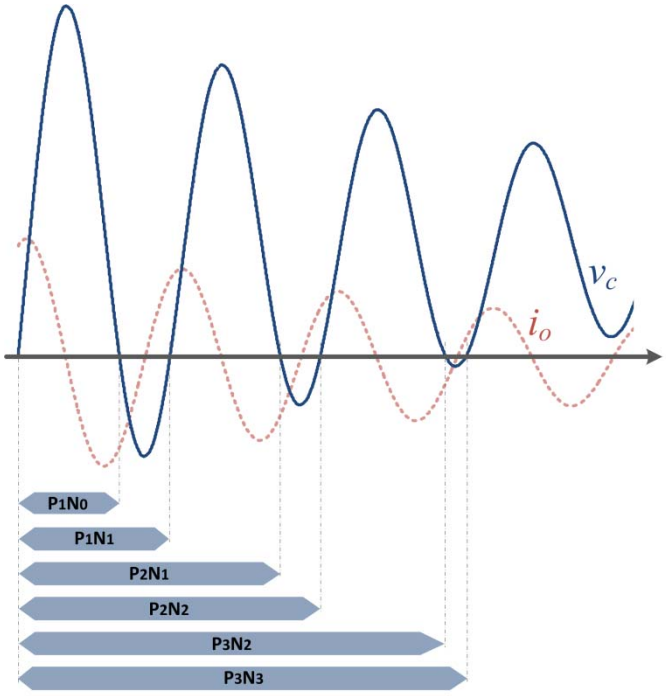

Fig. 8. Temporal waveforms of the resonant capacitor voltage and load current for different multi-cycle operation modes.

switch operation mode (P_1N_0), the switch activation pattern is {11} in State I, whereas the switch activation pattern is {01} for State II. Activation pattern {01} ensures the correct ZVS switching-on transition caused by the equivalent anti-parallel diode (it is activated when device voltage reaches zero). Once diode starts conducting, the switching device can be completely activated (state {11}) to reduce conducting loses, using the bidirectional current flow property of FET devices.

In the case of multi-cycle mode P_1N_1, the switching device activation pattern is {01} for state I and {00} for the State II. Thus, the equivalent parallel diode ensures the correct soft-switching ZVS turn-on transition. In this point, device conduction efficiency can be improved by using activation pattern {11} once diode starts conducting.

Finally, more complex multi-cycle modulations require a higher number of transitions for the equivalent switching device. For example, P_2N_1, (Fig. 9.c) requires a minimum of three changes to ensure ZVS turn-on transition. Note that only one equivalent switching device activation bit is changed in every transition.

As it has been done for the classical operation mode, the design plane for the multi-cycle operation modes is shown in Fig. 10 for a load quality factor, Q= 8 As it is shown, higher order multi-cycle modulation schemes reduce the required switching frequency for the same output power level, reducing switching losses and decreasing driver requirements. Moreover, the device peak voltage is also reduced depending on the multi-mode operation mode

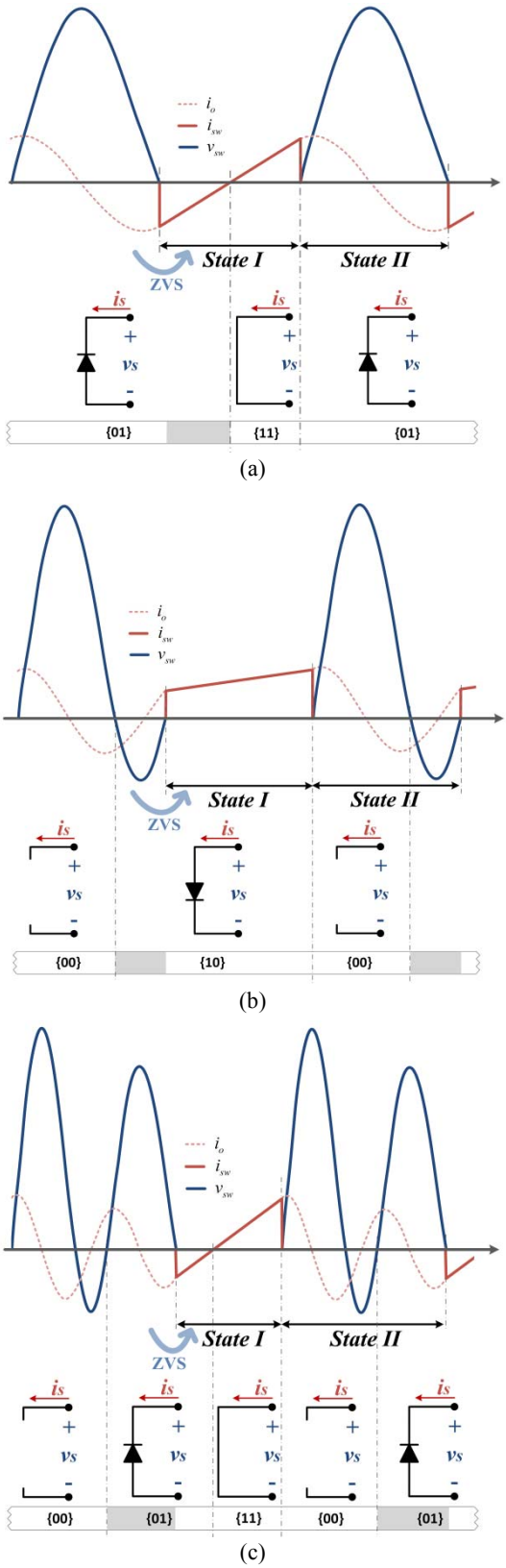

Fig. 9. Activation pattern for different multi-cycle operation mode. Conventional mode, P_1N_0 (a). Mode P_1N_1 (b). Mode P_2N_1 (c).

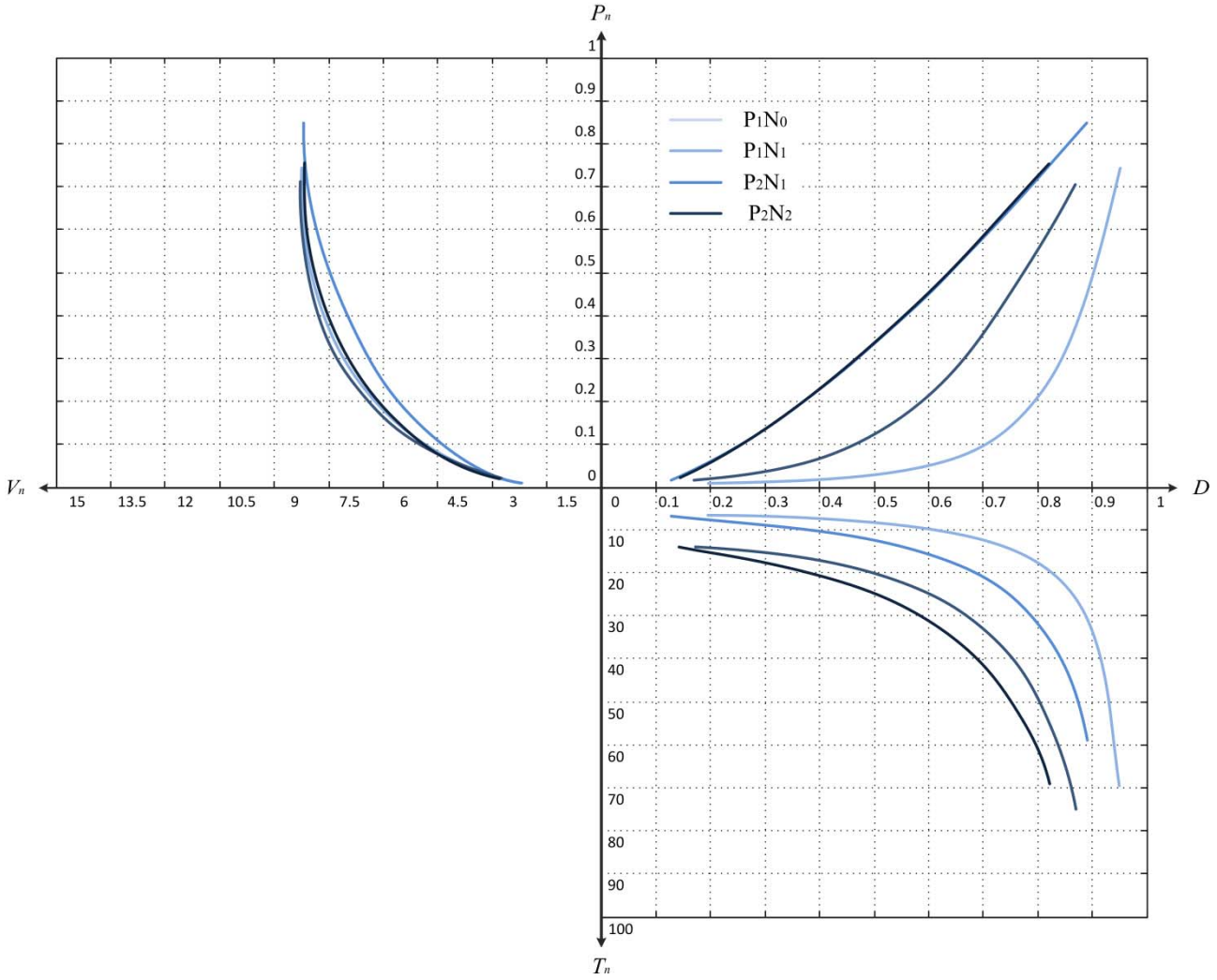

Fig. 10. Design map for different multi-cycle operation modes in the case of a load quality factor, Q=8.

As it is shown in Fig. 10 the best peak voltage reduction is achieved for the P_1N_1 modulation.

IV. Experimental Results

A power converter prototype (Fig. 11) for domestic induction heating purposes has been built to verify the feasibility of the proposed direct ac-ac converter. The induction load is modeled as the series connection of an equivalent resistor R_{eq} and an equivalent inductor L_{eq} [27]. The equivalent load resistance value is 2.82 Ω and the equivalent series inductance is 18 µH. The resonant capacitor has been set to 24 nF, leading to a load quality factor, Q, close to 8. This value is suitable to allow multiple multi-cycle operation modes. The SJEP120R063, SiC n-Channel normally-OFF JFETs have been used as switching devices [28]. Their reduced on-state resistance (63 mΩ at 25ºC) and switching losses make them suitable for the proposed domestic induction heating application. Although JFETs are bidirectional switching devices, antiparallel auxiliary SiC diodes have been used to ensure the correct ZVS turn-on sequence and protect devices against negative voltages. Main converter parameters are shown in Table II. The power converter is controlled by a Xillinx XCS3500E FPGA, and the mains supply voltage is sampled to perform the correct driving signals for the proposed direct ac-ac converter.

Table II
Prototype Parameters

	Components	Values
R_{eq}	IH load equivalent resistance	2.82 Ω
L_{eq}	IH load equivalent inductance	18 µH
C_r	Resonant capacitor	24 nF
V_{ac}	Mains supply voltage	120 V, 60 Hz
S_P, S_N	SiC JFET switching device	SJEP120R063
D_P, D_N	SiC antiparallel diodes	C4D05120E

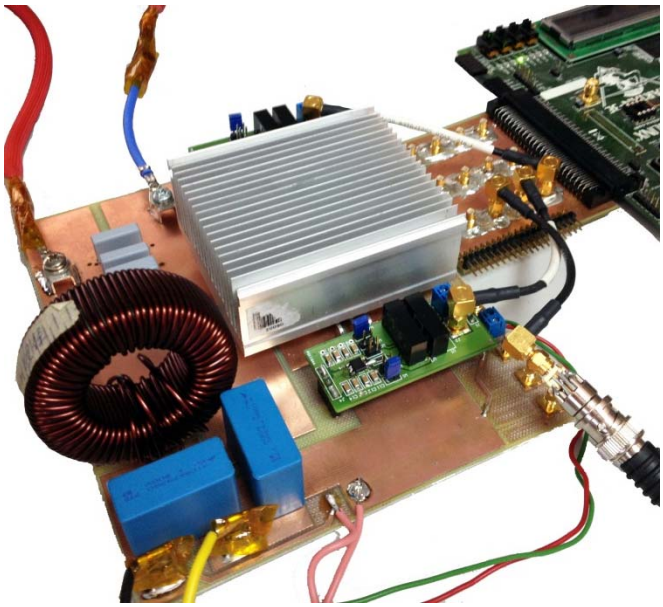

Fig. 11. Experimental prototype of the proposed direct ac-ac converter.

Considering the classical modulation strategy (P_1N_0), the optimum operation mode is achieved at 210 kHz (Fig. 12(a)). The output power is increased by reducing the switching frequency and operating the converter in the sub-optimum operation mode (Fig. 12.b). Fig. 13 and Fig. 14 show the multi-cycle modulations P_1N_0 and P_2N_2, respectively, proving the feasibility and proper operation of MCMs in the proposed converter. In Fig. 13, the driving signals generation according to the mains voltage sign can be also seen, whereas in Fig. 14 shows a more complex MCM that allows improving output power control. The most relevant multi-cycle modulations have been experimentally verified and plotted in Fig. 15 to verify the entire output power range. One important conclusion is that the same output power can be delivered within a wide range of switching frequencies. This is especially important for domestic induction heating systems, where recent multi-load designs [13] require distant switching frequencies to avoid acoustic intermodulation noise. For example, the implemented converter can deliver 250-W output power in a range from 45 kHz in mode P_3N_3 to 125 kHz in P_1N_1 operation mode, avoiding the intermodulation acoustic bandwidth (20 kHz).

V. Conclusions

In this paper, a class-E direct ac-ac converter featuring multi-cycle modulation scheme has been proposed for induction heating systems. The proposed converter avoids the need of a rectifier stage, reducing the number of components, complexity, and conduction losses.

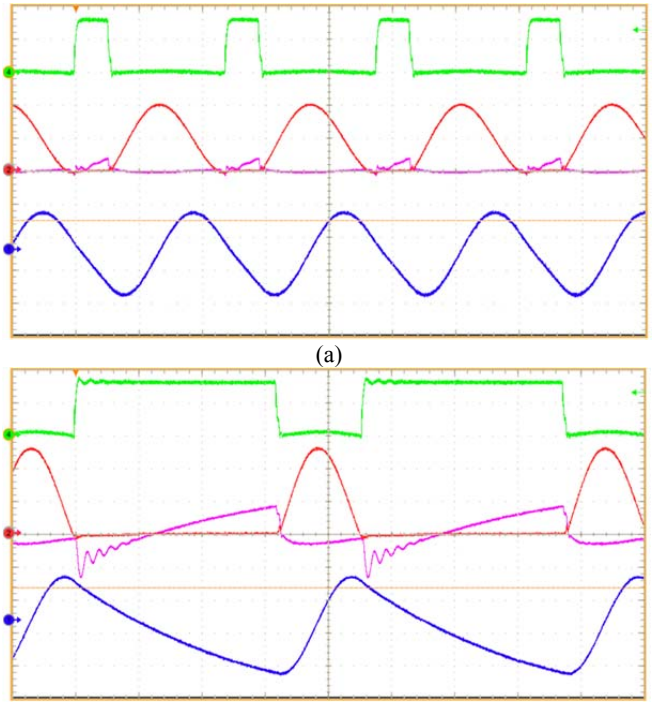

(a)

(b)

Fig. 12. Key waveforms for the classical modulation. Waveforms for the optimum ZVDS at 210 kHz (a) and for sub-optimum ZVS mode at 110 kHz (b). From top to bottom: positive switching device activation signal (10 V/div); switch voltage (200 V/div) and current (15 A/div); load current (20 A/div).

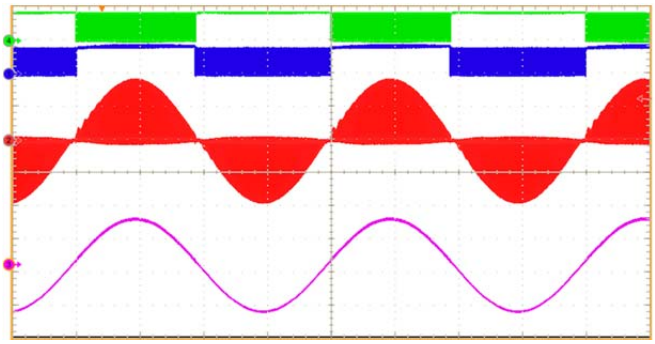

Fig. 13. Direct ac-ac converter operated at P_1N_0 (f_{SW}=200 kHz). From top to bottom: positive and negative switching device activation signals (20 V/div); equivalent switch voltage (200 V/div); mains supply voltage (50 V/div).

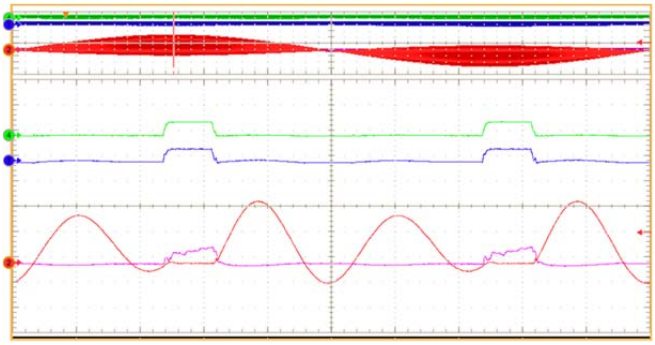

Fig. 14. Operation at P_2N_2 (f_{SW}=100 kHz). From top to bottom: switching device activation signals (20 V/div); equivalent switch voltage (200 V/div); and current (20 A/div).

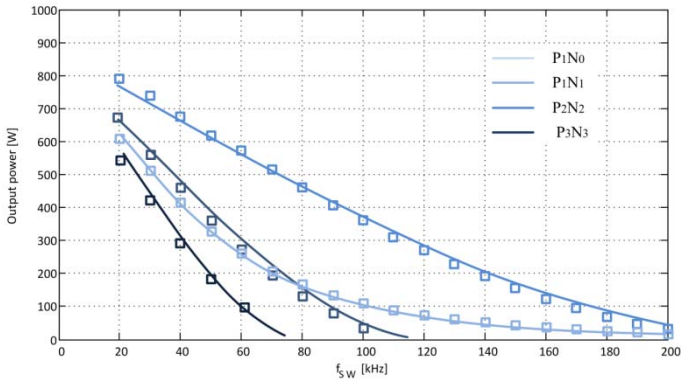

Fig. 15. Theoretical (line) and experimental results (square dots) output power plane as a function of the switching frequency for different multi-cycle modulation schemes.

Moreover, multi-cycle modulation scheme allows reducing the peak voltage and improving output power control capabilities, which are the main drawbacks of classical class-E implementations for induction heating systems.

The proposed converter has been tested using SiC JFET devices, which perfectly fit this application. Experimental measurements agree with the expected analytical results and prove the feasibility of the proposed converter. As a conclusion, the proposed class-E direct ac-ac converter with multi-cycle modulations is proposed to further improve the performance of induction heating systems in the medium-low output power level.

REFERENCES

[1] Y. Song and B. Wang, "Survey on reliability of power electronic systems," *IEEE Transactions on Power Electronics,* vol. 28, pp. 591-604, January 2013.

[2] W. Feng, F. C. Lee, and P. Mattavelli, "Optimal trajectory control of burst mode for LLC resonant converter," *IEEE Transactions on Power Electronics,* vol. 28, pp. 457-466, January 2013.

[3] H. W. Koertzen, J. A. Ferreira, and J. D. van Wyk, "A comparative study of single switch induction heating converters using novel component effectivity conceps," in *IEEE Power Electronics Specialists Conference*, 1992, pp. 298-305.

[4] Y. Kawaguchi, E. Hiraki, T. Tanaka, and M. Nakaoka, "Full bridge phase-shifted soft switching high-frequency inverter with boost PFC function for induction heating system," in *European Conference on Power Electronics and Applications*, 2007, pp. 1-8.

[5] D. Czarkowski and M. K. Kazimierczuk, "Single-capacitor phase-controlled series resonant converter," *IEEE Transactions on Circuits and Systems,* vol. 40, pp. 383-391, June 1993.

[6] V. Esteve, E. Sanchis-Kilders, J. Jordan, E. J. Dede, C. Cases, E. Maset, J. B. Ejea, and A. Ferreres, "Improving the efficiency of IGBT series-resonant inverters using pulse density modulation," *IEEE Transactions on Industrial Electronics,* vol. 58, pp. 979-987, March 2011.

[7] S. Chudjuarjeen, A. Sangswang, and C. Koompai, "An improved LLC resonant inverter for induction-heating applications with asymmetrical control," *IEEE Transactions on Industrial Electronics,* vol. 58, pp. 2915-2925, July 2011.

[8] A. Fujita, H. Sadakata, I. Hirota, H. Omori, and M. Nakaoka, "Latest developments of high-frequency series load resonant inverter type built-in cooktops for induction heated all metallic appliances," in *IEEE Power Electronics and Motion Control Conference*, 2009, pp. 2537-2544.

[9] H. W. Koertzen, J. D. v. Wyk, and J. A. Ferreira, "Design of the half-bridge series resonant converters for induction cooking," in *IEEE Power Electronics Specialist Conference Records*, 1995, pp. 729-735.

[10] O. Lucía, J. M. Burdío, I. Millán, J. Acero, and L. A. Barragán, "Efficiency oriented design of ZVS half-bridge series resonant inverter with variable frequency duty cycle control," *IEEE Transactions on Power Electronics,* vol. 25, pp. 1671-1674, July 2010.

[11] O. Lucía, J. M. Burdío, I. Millán, J. Acero, and D. Puyal, "Load-adaptive control algorithm of half-bridge series resonant inverter for domestic induction heating," *IEEE Transactions on Industrial Electronics,* vol. 56, pp. 3106-3116, August 2009.

[12] M. Fujun, L. An, X. Xianyong, X. Huagen, W. Chuanping, and W. Wen, "A Simplified Power Conditioner Based on Half-Bridge Converter for High-Speed Railway System," *IEEE Transactions on Industrial Electronics,,* vol. 60, pp. 728-738, 2013.

[13] O. Lucía, J. M. Burdío, L. A. Barragán, J. Acero, and I. Millán, "Series-resonant multiinverter for multiple induction heaters," *IEEE Transactions on Power Electronics,* vol. 24, pp. 2860-2868, November 2010.

[14] H. Fujita, N. Uchida, and K. Ozaki, "A new zone-control induction heating system using multiple inverter units applicable under mutual magnetic coupling conditions," *IEEE Transactions on Power Electronics,* vol. 26, pp. 2009-2017, July 2010.

[15] Y.-C. Jung, "Dual half bridge series resonant inverter for induction heating appliance with two loads," *Electronics Letters,* vol. 35, pp. 1345-1346, May 1999.

[16] H. Pham, H. Fujita, K. Ozaki, and N. Uchida, "Phase angle control of high-frequency resonant currents in a multiple inverter system for zone-control induction heating," *IEEE Transactions on Power Electronics,* vol. 26, pp. 3357-3366, 2011.

[17] H. Sarnago, O. Lucía, A. Mediano, and J. M. Burdío, "Class-D/DE dual-mode-operation resonant converter for improved-efficiency domestic induction heating system," *IEEE Transactions on Power Electronics,* vol. 28, pp. 1274-1285, 2013.

[18] J. I. Rodriguez and S. B. Leeb, "A multilevel inverter topology for inductively coupled power transfer," *IEEE Transactions on Power Electronics,* vol. 21, pp. 1607-1617, 2006.

[19] J. I. Rodriguez and S. B. Leeb, "Nonresonant and resonant frequency-selectable induction-heating targets," *IEEE Transactions on Industrial Electronics,* vol. 57, pp. 3095-3108, September 2010.

[20] I. Hirota, H. Omori, K. A. Chandra, and M. Nakaoka, "Practical evaluations of single-ended load-resonant inverter using application-specific IGBT and driver IC for induction-heating appliance," in *Proceedings of 1995 International Conference on Power Electronics and Drive Systems* 1995, pp. 531-537 vol.1.

[21] J. Acero, C. Carretero, R. Alonso, O. Lucía, and J. M. Burdío, "Mutual impedance of small ring-type coils for multi-winding induction heating appliances," *IEEE Transactions on Power Electronics,* vol. 28, pp. 1025-1035, February 2013.

[22] C. Carretero, O. Lucía, J. Acero, and J. M. Burdío, "Computational modeling of two partly-coupled coils supplied by a double half-bridge resonant inverter for induction heating appliances," *IEEE Transactions on Industrial Electronics,* vol. x, p. x, x 2013.

[23] N. O. Sokal, "Class E high-efficiency switching-mode tuned power amplifier with only one inductor and one capacitor in load network-approximate analysis," *IEEE Journal of Solid-State Circuits,* vol. 16, pp. 380-384, 1981.

[24] H. Sarnago, O. Lucía, A. Mediano, and J. M. Burdío, "Modulation scheme for improved operation of a RB-IGBT based resonant inverter applied to domestic induction heating," *IEEE Transactions on Industrial Electronics,* 2013.

[25] N. A. Ahmed, "High-frequency soft-switching ac conversion circuit with dual-mode PWM/PDM control strategy for high-power IH applications," *IEEE Transactions on Industrial Electronics,* vol. 58, pp. 1440-1448, April 2011.

[26] A. L. Shenkman, "Transient Analysis of Electric Power Circuits Handbook," *Springer,* The Netherlands, 2005.

[27] J. Acero, C. Carretero, I. Millán, O. Lucía, R. Alonso, and J. M.

Burdío, "Analysis and modeling of planar concentric windings forming adaptable-diameter burners for induction heating appliances," *IEEE Transactions on Power Electronics,* vol. 26, pp. 1546-1558, May 2011.

[28] J. Rabkowski, G. Tolstoy, D. Peftitsis, and H. Nee, "Low-loss high-performance base-drive unit for SiC BJTs," *IEEE Transactions on Power Electronics,* vol. 27, pp. 2633-2643, May 2012.